Teravoxel Microscopy Image Analysis for Neurological Diseases

Ziquan Wei,[1] and Guorong Wu[1,2,3]

[1]Department of Computer Science
[2]Department of Psychiatry
[3]Neuroscience Center, University of North Carolina at Chapel Hill, Chapel Hill, USA, 27599; email: grwu@med.unc.edu

Annual Review of Biomedical Engineering YYYY. AA:1–23

https://doi.org/10.1146/((please add article doi))

Copyright © YYYY by the author(s). All rights reserved

Keywords

light sheet fluorescence microscopy, neurological disease, volumetric image analysis, machine learning

Abstract

Light sheet fluorescence microscopy (LSFM) has emerged as a revolutionary imaging modality for investigating intact three-dimensional brain structures at the teravoxel scale. In parallel, high-throughput computational methods, especially deep learning approaches, have opened new avenues for uncovering the pathophysiological mechanisms of neurological diseases through LSFM technology. Recent advances in optics and tissue clearing methods have allowed whole-brain imaging at cellular resolution in three dimensions, and the integration of artificial intelligence (AI) has facilitated the identification of disease-related cellular profiles and morphological markers. Machine learning techniques for stitching, segmentation, classification, super-resolution, and registration, therefore, are promoted to uncover biological patterns that are not visible to human eyes, yet related to neuroinflammatory and neurodegenerative diseases. However, analytic pipelines have been designed differently for various animal models and brain structures, leading to challenges in feasibility and compatibility within this emerging field of data-driven LSFM image analysis. Here, we present an overview of current pipelines, examine existing and forthcoming challenges as the LSFM community advances, demonstrate their implications for neurological disease applications, and propose potential solutions.

Contents

1. INTRODUCTION

As we enter the era of artificial intelligence (AI), AI for neurological diseases shows great potential for computer-aided prognosis (1, 2), diagnosis (3), and therapeutics (4). The past decades have witnessed diverse neurological applications of AI and machine learning, focusing on magnetic resonance imaging (MRI), electroencephalogram (EEG), transcriptomic, metabolomic, phenotypic data, and microscopy image analysis (5). In contrast, microscopy imaging techniques are not widely used for the investigation of early-stage neurological diseases, as the acquisition of suitable brain tissue is invasive and carries a significant risk (6). This is reflected by the large difference in publication numbers in neurology of 82 versus 2,420 on the topic of microscopy and MRI for neurology, respectively[1]. However, microscopy reveals structural details linked to neurological diseases, which non-invasive methods are struggling with in terms of resolution and specificity. Investigating disease-related structural changes in the nervous system requires imaging heterogeneous structures at vascular, cellular, and subcellular scales across subject populations. For example, alterations in the cerebrovascular system serve as a possible marker of Alzheimer's disease (AD), as early changes in blood vessels are directly associated with tau pathology (7).

The parallel development and maturation of public datasets have fueled the neurological analysis revolution, providing access to longitudinal and multimodal data, including MRI, EEG, phenotypes, and genotypes (8, 9, 10, 11). Diverse innovations in unified standards in the preprocessing of whole-brain data (12, 13) attract interests in machine learning, e.g., large-scale modeling (14, 15) and structure-function coupling (16, 17), for neurodegeneration. Nonetheless, microscopy is increasingly being adopted as an alternative modality to satisfy the desire to see structural details in specific neurons. In early studies, cell localization and structure segmentation within brain sections, e.g., detecting cells stained for the somatostatin receptor based on confocal fluorescence microscopy (18), suggest new strategies for the treatment of neurological and psychiatric disorders from microscopy. On the other hand, another modality, bright field

[1]Conducted on November 3, 2025, using searching strings '(MRI[Title/Abstract]) AND (neurology[Title/Abstract])' and '(microscopy[Title/Abstract]) AND (neurology[Title/Abstract])' for MRI-related and microscopy-related articles, respectively, on page `https://pubmed.ncbi.nlm.nih.gov/`

microscopy images, has been curated and released as part of the Cancer Genome Atlas (TCGA) database for the detection of glioblastoma multiforme (GBM) in brain sections (19). Although the quantity of brain studies based on the TCGA dataset—1,343 articles in PubMed[2]—is growing, this type of microscopy image analysis still studies a partial brain. The whole-brain analysis for neurological diseases is based on a new modality.

Although light sheet fluorescence microscopy (LSFM) and three-dimensional (3D) tissue clearing were present more than 100 years ago (20, 21), a guinea-pig cochlea was imaged by the first integration of tissue clearing and LSFM after approximately 90 years (22). Brain LSFM was then present in the 2000s as a breakthrough that enabled, for the first time, 3D cellular-level mapping of complete neuronal architectures in intact mouse brains, marking a pivotal moment in whole-brain imaging (23). Afterward, initial attempts of machine learning approaches that analyze whole-brain LSFM have been made on local structures, e.g., neuronal arbor segmentation (24). However, LSFM imaging of the whole brain introduces $10^4\times$ more voxels than non-invasive neuroimaging, adding challenges of stitching, visualization, and registration to machine learning in such a teravoxel volumetric image for cell and structure profiling (25, 26). Although teravoxel image analysis in the volume electron microscopy modality characterizes the ultrastructure of the brain, including synapses (27) and axons (28), the existing study (28) for neurological diseases is based on 3D gigavoxel images around local patches without scaling up to the whole brain. Therefore, in this review of teravoxel microscopy image analysis for neurological diseases, the term 'teravoxel' specifically refers to LSFM. Here, we explain the basic principle of teravoxel image analysis in the era of AI and its unique benefits and challenges over non-invasive neuroimaging for neurological diseases. The evolution of teravoxel microscopy image analysis is then reviewed, with a focus on profiling the entire mammalian brain. We then discuss the promise of neurology studies powered by teravoxel image analysis based on whole-brain neuron morphology on the cellular scale.

2. AI FOR NEUROLOGICAL DISEASES

The convergence of AI for neurological diseases represents a transformative paradigm in neuroscience. Traditional computational approaches in neurology are based on preprocessing frameworks for *in vivo* neuroimaging (Fig. 1a,b), allowing unprecedented characterization of disease-related alterations in regional signal, averaged surface, and connectivity. Advanced deep learning frameworks, including convolutional neural networks (Fig. 1c), and graph neural networks (Fig. 1d), have demonstrated remarkable capabilities in neurological applications, such as brain-to-stimuli decoding (29) and human connectome analysis (17).

The integration of high-resolution imaging technologies with AI represents this shift toward large-scale image analysis for neurological disease. LSFM generates teravoxel-scale datasets that capture cellular-level detail across entire brain volumes (Fig. 1e), providing opportunities for AI-driven analysis of neurological pathology. Pipelines are computationally heavier on whole-brain microscopy than non-invasive neuroimaging due to the additional steps handling exponentially increased data scale and profiling fundamental structures across the entire neural system, e.g., neuron (30) and blood vessel (25). These technological developments enable quantitative assessment of neuronal morphology, synaptic connectivity, and vascular distributions with spatial precision previously unattainable through *in vivo* neuroimaging.

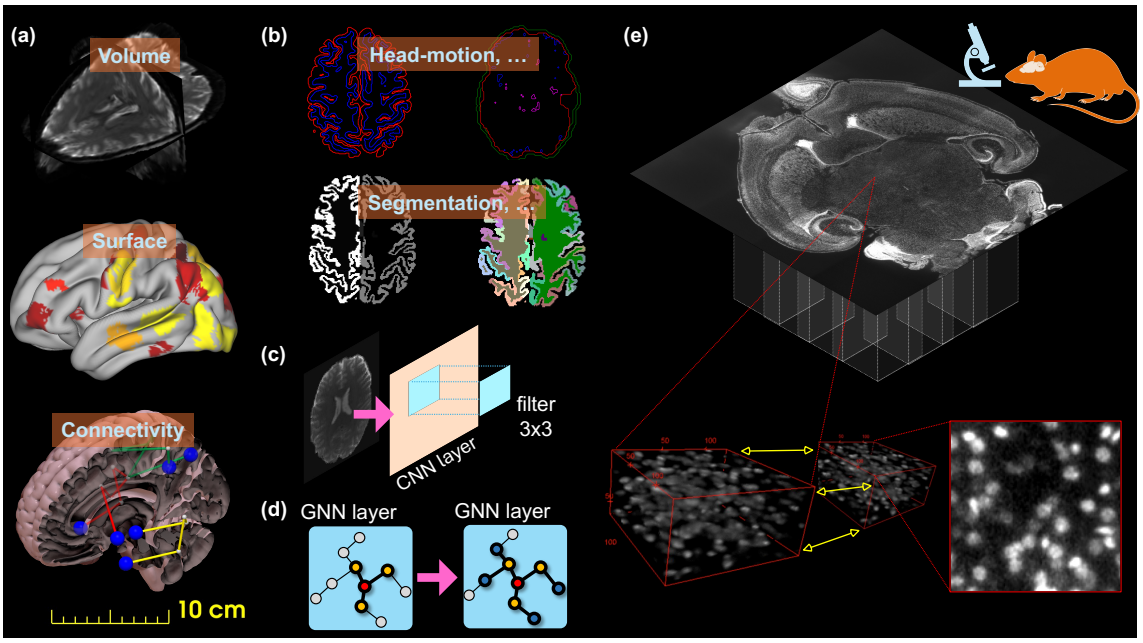

Figure 1

AI for neurological diseases based on non-invasive neuroimaging and teravoxel imaging. (a) Three data modalities of AI for *in vivo* neuroimaging, adapted from (17). (b) Two example preprocessing steps for non-invasive neuroimaging to generate multimodal data, adapted from (17). (c) Convolutional Neural Networks (CNN) for volume modality, adapted from (17). (d) Graph Neural Networks (GNN) for connectivity modality, adapted from (31). (e) The teravoxel imaging, where yellow arrows indicate the preprocessing step of 3D reconstruction, is adapted from (32).

Table 1 Comparison of signal-to-noise ratio (SNR) definitions across neuroimaging modalities.

Modality	MRI	PET	CT	LSFM
SNR=	$\frac{mean(\text{Signal in ROI})}{std(\text{Noise})}$ (33)	$\frac{mean(\text{Lesion})-mean(\text{Background})}{std(\text{Background})}$ (34)	$\frac{mean(\text{Signal})}{std(\text{Noise})}$ (35)	$\frac{\mu}{\sigma}$ (36)

Note. ROI = region of interest; μ and σ represent the mean and standard deviation of voxel intensities in LSFM images, respectively.

2.1. Limited Resolution and SNR of in vivo Neuroimaging

Non-invasive neuroimaging modalities, including MRI, positron emission tomography (PET), and computed tomography (CT), present inherent constraints in spatial resolution and signal-to-noise ratio (SNR) that can limit their ability to comprehensively characterize neurological disease (37, 38). The quantitative definitions of SNR for representative neuroimaging and microscopy modalities are summarized in Table 1, where non-invasive methods average signals among regions of interest. These techniques generally achieve resolutions ranging from millimeters to centimeters (39), which are coarser than the sizes of individual neurons ($10\sim100\mu m$ soma) or synapses ($1\sim2\mu m$), resulting in that MRI/PET/CT cannot directly resolve

[2]Conducted on November 7, 2025, using the searching string '(TCGA[Title/Abstract]) AND (brain[Title/Abstract])' on page `https://pubmed.ncbi.nlm.nih.gov/`

cellular or synaptic detail. For example, diffusion tensor imaging (DTI) might not show subtle preclinical neuronal loss (40).

Machine learning approaches applied to non-invasive neuroimaging data must contend with fundamental physical constraints such as limited resolution and low signal-to-noise ratio (SNR), necessitating standardized preprocessing and feature extraction pipelines to extract biologically meaningful signals from noisy measurements (12, 41). These preprocessing steps, including denoising, head-motion correction, tissue segmentation, and regional averaging (Fig. 1b), are widely adopted in studies and form the foundation for downstream machine learning analyzes. They typically produce standardized data representations, i.e., volumetric, surface, or connectivity forms (Fig. 1a), upon which specialized models such as convolutional neural networks (CNNs) and graph neural networks (GNNs) are built (Fig. 1c–d). These representations enable quantitative characterization of regional tissue properties while maintaining anatomical correspondence with a predefined atlas (42).

Building on these standardized data representations, recent advances have leveraged AI-driven multimodal frameworks to partially overcome the limitations imposed by resolution and SNR. By integrating complementary information from multiple non-invasive modalities, multimodal frameworks enhance sensitivity to early disease-related changes that are imperceptible in single-modality analyzes (43). Notable applications include the early detection of neurodegenerative disorders, where multimodal methods achieve diagnostic accuracy exceeding 90% for Alzheimer's disease by combining MRI and PET (44), and improved modeling of structure-function relationships in the human brain (16, 17). On the other hand, graph neural networks (GNNs) have emerged as powerful tools to mitigate the analytical impact of limited resolution and SNR by modeling geometry and connectivity patterns rather than individual voxels from neuroimaging (45, 46). As illustrated in Fig. 1d, GNNs propagate information through the structural or functional geometry of the brain to capture complex topological dependencies within brain networks. Thereby, it enhances robustness to voxel-wise noise (47) and enables the detection of subtle connectivity disruptions that may be undetectable using conventional statistical or non-learnable methods (48). Recent attention-based GNN variants further improve diagnostic precision in psychiatric disorders such as depression and schizophrenia (49, 50).

However, the underlying resolution limitations of non-invasive neuroimaging modalities may continue to constrain the capacity of even the most advanced AI architectures to provide cellular-level insights that could be essential for understanding the mechanisms of neurological disease mechanisms (51). Although computational approaches can extract maximum information from available data, the fundamental physical constraints of these *in vivo* techniques establish an upper bound on the biological detail accessible through image analysis.

2.2. Whole-Brain LSFM: Gold Standard Data

Light-sheet fluorescence microscopy (LSFM) represents a shift in neuroscience imaging, providing unprecedented access to the cellular architecture with subcellular resolution (Fig. 1e) across entire organ systems, e.g., the brains of zebrafish (52) and mouse (53). This advanced optical technique, cooperating with tissue clearing, generates teravoxel-scale datasets ($>10^{12}$ voxels per brain volume) that capture neuronal morphology, connectivity patterns, and vascular distributions with spatial resolutions approaching sub-micrometer, superior to non-invasive neuroimaging approaches (54, 55). Fig. 1e shows an example of a whole-brain imaging of a mouse adapted from the paper (32). Tiling of the entire brain is necessary when the specimen is large, as indicated by multiple stacks in Fig. 1e, leading to a stitching step for neighboring tiles as yellow arrows to reconstruct the complete 3D specimen.

The fundamental advantage of LSFM lies in its ability to illuminate thin optical sections ($1\sim5$ μm thickness) through the sample using light sheets, thus minimizing phototoxicity and photobleaching while

maintaining high-speed acquisition capabilities (1∼10 Hz volume rates) (56, 53, 57), compared to days for confocal microscopy (58). This approach enables comprehensive 3D reconstruction of entire brain volumes (up to 1 cm^3), preserving spatial relationships between diverse cell populations and their associated pathological features (59). For neurological disease research, LSFM datasets provide direct access to pathological protein aggregates (e.g., amyloid plaques and neurofibrillary tangles (60)), synaptic alterations (61), cellular degeneration (30), and vascular morphology patterns (25) that remain invisible to conventional imaging modalities (62, 63).

The high resolution, e.g., 450nm laterally and 2um axially (52), and high SNR, e.g., 1000:1 (53), characteristics of the LSFM data establish these datasets as gold standard references for understanding the progression of neurological disease (64, 65). Unlike *in vivo* analysis that relies on indirect measurements of brain function or structure through hemodynamic responses or tissue contrast, LSFM provides direct access to cellular and molecular-level pathology (58). This capability proves particularly valuable for investigating neurodegenerative diseases, where understanding the spatial distribution and temporal evolution of protein misfolding, neuroinflammation, and synaptic loss is crucial for the development of targeted therapeutic strategies (66, 67).

2.3. AI-based Analysis Profiles Whole-Brain Morphology

The analysis of these enormous LSFM volumetric images has been revolutionized by deep learning. Modern pipelines use CNNs and related architectures to automatically segment and quantify cellular, subcellular, or vascular structures throughout the brain (68, 69). For example, 3D U-Net (70) has been applied to zebra fish neuron (68) and mouse vasculature data (25) based on LSFM images.

Deep learning (DL) approaches excel at identifying subtle morphological alterations in neuronal populations that can indicate early pathological changes in neurological diseases (71). Early studies like BigNeuron (72) and DeepNeuron (73) can automatically segment neurons, dendrites, and axonal projections across entire brain regions with a precision matching human expert annotations (Dice coefficients >0.9), enabling statistical analysis of cellular morphometric parameters including soma volume, dendritic branching complexity (Sholl analysis), spine density, and axonal integrity. Although these early results are patch-based, such quantitative phenotyping capabilities are essential to understand how neurological diseases affect specific cellular populations and neural circuits (74).

The computational efficiency and patch result stitching of this teravoxel image analysis task are a pivotal factor in the feasibility of whole-brain profiling. Although human equivalent performance is observed in recognizing cropped image patches, reconstructing the cropped results as a whole brain is a necessary step. Studies transfer the problems as voxel-wise prediction and grouping so that the computation time ranges from hours to days per brain, and the patch-based results can be concatenated as the whole brain directly (30, 75). As a result, cell count and vessel size can be quantified in the brain (30, 25).

Aside from the automatic algorithms, manual annotations are the basis for data-driven AI. The interactive frameworks, such as ilastik (76) and segmentor (77), provide multiple annotation modes to facilitate a wide range of applications, from voxel-wise annotation to 3D object tracking. Advanced self-supervised and contrastive learning methods are also being incorporated to reduce annotation needs in LSFM. Techniques like a simple framework for contrastive learning (78) or masked autoencoders (79) allow networks to pre-train on unlabeled brain images and then fine-tune on limited hand-annotated samples. This reduces the manual labeling burden (50-80%) while maintaining accuracy (69). Advanced annotation tasks such as manual stitching are challenging in LSFM because of imaging uncertainties arising from environmental and experimental factors (80). For example, movement and vibration of the imaging device, refractive-index heterogeneity, uneven illumination of the light sheet, and variability in tissue clearing can reduce registration accuracy and complicate manual alignment. Software for stitching purposes, e.g., TeraStitcher (81)

and Imaris (82), is rare but has been developed to fulfill the needs of interactively visualizing the teravoxel image with the function of shifting 3D tile images for manual stitching.

3. THE EVOLUTION OF TERAVOXEL IMAGE ANALYSIS

The integration of deep learning methodologies with teravoxel LSFM datasets has refreshed our capacity to extract quantitative insights from complex neurobiological structures across multiple resolution scales (54, 83). Whole-brain computational frameworks enable comprehensive profiling of vascular networks, cellular populations, and subcellular components through automated analysis pipelines that process whole-brain imaging volumes with precision and throughput (59, 84). The evolution of such huge volumetric data analysis starts from smaller sizes and fewer data, namely, gigapixel whole-slide images (Fig. 2c), before the computational hardware is capable of the scale of teravoxel. Although pipelines for 3D teravoxel images analysis (Fig. 2m) differ from 2D (Fig. 2l), computer vision (CV, which refers broadly to computational approaches for automated image analysis, encompassing both traditional image-processing techniques and modern deep learning-based methods) tasks are as same as 2D (Fig. 2fgh) for local patches in 3D (Fig. 2ij). In this section, the evolution of teravoxel microscopy image analysis for neurological diseases is reviewed from where it started to the state-of-the-art (SOTA) pipelines.

3.1. Early Neurological Studies for Gigapixel Microscopy Image Analysis

The foundational trajectory of large-scale biological image analysis originated from pioneering developments in bright field microscopy (BFM) imaging systems, establishing the computational precedent for whole-slide imaging applications of images larger than megapixel natural images (87, 88). Early work in computational pathology applied automated analysis to tissue microarrays (TMA), which consist of arrays of megapixel microscopy images (89). The analysis represents antecedents of modern cell-detection methods applied to large bright-field microscopy (BFM) images (e.g., 3000×3000 pixels), substantially larger than typical natural-image datasets.

As shown in Fig. 2abcd, although LSFM existed as dark-field microscopy more than 100 years ago, cell profiling became feasible for BFM gigapixel imaging earlier than LSFM imaging when computers were equipped with gigabytes of memory. Aperio's BigTIFF-enabled scanners first supported gigapixel slide imaging in a practical and production-grade setting in 2007. As semi-supervised learning (90) and unsupervised learning (91) for pathology images have not been presented, computer vision (CV) tasks for pathology images were focused on local patches with manual annotations instead of the entire gigapixel image. The methods for image classification (Fig. 2f), object detection (Fig. 2g), and instance segmentation (Fig. 2h) have evolved from handcrafted feature-extraction approaches (92, 93) to modern DL-based methods (94, 95) for accurate local patch recognition.

As computational efficiency grows in the deep learning era, CNN was adapted to a complete gigapixel whole slide image (WSI) analysis in 2016 (96) for the GBM prediction of WSIs in the TCGA dataset. This brings a general pipeline (Fig. 2l) in 2D WSI analysis by acting like pathologists, (i) finding diseased local patches, then (ii) summarizing reports or labeling based on detected patches (97, 98). Subsequently, tile-based decomposition strategies divided large gigapixel-scale brain sections into smaller, more manageable subregions, which maintained spatial continuity by using predefined overlapping boundary regions (99).

Following these CV and gigapixel advances in 2D, deep learning algorithms constituted the core analytical component. Taupathologies are the main focus of gigapixel image analysis for neurological diseases. For example, in patch-level recognition, (100) implemented residual network (ResNet) (101) based pyramid scene parsing networks (102) for pTau and pTDP-43 segmentation, where the model demonstrated intersection over union (IoU) exceeding 60%. Similarly, a fully convolutional network is applied by (103)

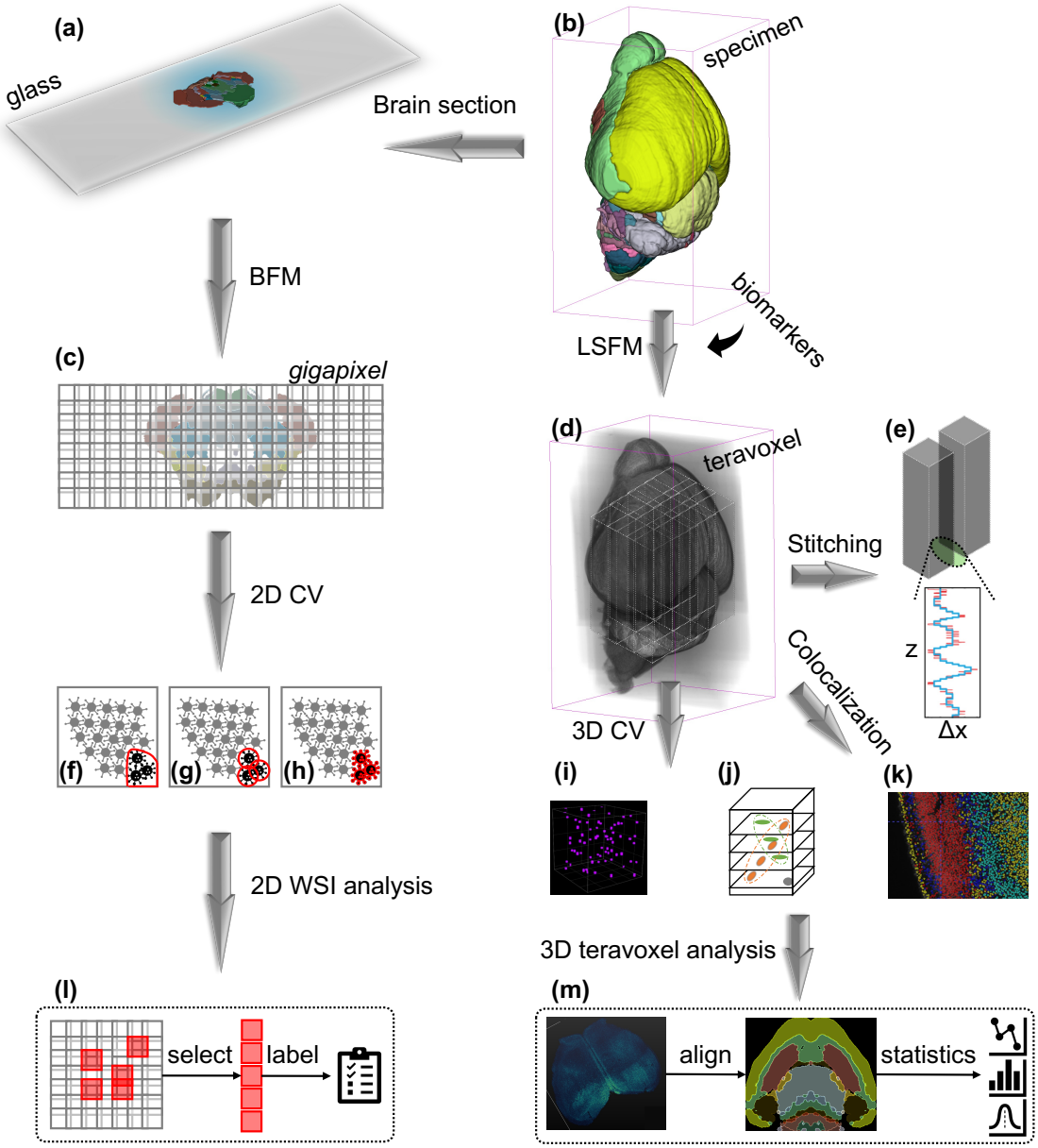

Figure 2

The typical workflows of teravoxel image analysis for neurology. (a) Brain section mounted on the glass, generated from CCFv3 atlas (85). (b) The specimen of a mouse brain, generated from CCFv3 atlas (85). (c) Gigapixel whole slide image (WSI), which is assembled from 2D tiles, generated from CCFv3 atlas (85). (d) Teravoxel whole brain LSFM image, which is assembled from 3D tiles, generated from CCFv3 volume (85). (e) An example of the preprocessing step, stitching, adapted from (86). 2D Computer Vision (CV) tasks have (f) pixel grouping, (g) object detection, and (h) instance segmentation. 3D CV tasks have (i) cell counting and (j) instance segmentation, adapted from (30) and (32), respectively. (k) Cell colocalization from multiple fluorescence channels. (l) 2D WSI analysis pipeline. (m) 3D teravoxel image analysis pipeline, the whole brain map is adapted from (32).

for tauopathy detection, achieving a 77-90% true positive ratio. Not long after, (104) utilized the pre-trained ResNet as a feature extractor to train a multilayer perceptron (MLP) for AD classification from tau immunostained WSI.

Although studies added more components to improve interpretability in local patch selection (91, 105), the principle of WSI analysis is still to conclude a result based on smaller regions of interest (RoI) from the brain section that is sliced off the whole brain. Given that the WSI is already a partial brain, selected patches or objects are hard to grab systematic whole-brain features for studying neuropathology. In the opposite, neurological diseases care about biomarkers and morphology across the intact brain to cover all interesting regions (104, 106). As the qualitative evidence of neuropathology present in an early BFM imaging study of AD (107), we can observe that neurological biomarkers are distributed across the whole brain. This urges the analysis of a teravoxel microscopy image of the whole brain.

3.2. Improvements to Microscopy Image Analysis Towards Teravoxel

The evolution from gigapixel whole-slide imaging to teravoxel volumetric analysis necessitates algorithmic frameworks capable of processing large-scale images that exceed the computational boundaries of gigapixel images by several orders of magnitude. This emerging field has different imaging workflows using LSFM rather than BFM, where specimen preparation (Fig. 2b) utilizing tissue clearing protocols and biomarker fluorescence precedes acquisition of intact tissue volume. Consequently, the computational infrastructure required to process these volumetric images has evolved from gigabyte memory architectures to terabyte memory due to vast interesting objects showing up in a 3D form with a clearer contrast between background and fluorescence excitation, as well as the elevated scale of voxel amount (108, 109).

The transformation from 2D WSI analysis to 3D volume analysis does not mirror the methodological evolution depicted in BFM imaging workflows, where teravoxel data (Fig. 2d) undergo additional stitching procedures (Fig. 2e) to generate an intact whole brain in 3D. Furthermore, colocalization is required for LSFM using multiple fluorescence channels to classify different cellular or molecular objects, e.g., upper-layer and lower-layer neurons (red and cyan colors in Fig. 2k). However, computational architectures specifically designed for 3D image analysis in the CV field have rarely been designed for the LSFM modality and the teravoxel scale.

The 3D CV objectives (Fig. 2ij) are a direct extension of the 2D CV tasks (Fig. 2gh) in most cases. Segmentation in 3D CV (Fig. 2j), for example, was first proposed by (110) for the confocal fluorescence microscopy image in 2007. This fully automated method for segmenting 3D cell nuclei is specifically designed to handle closely touching nuclei through gradient flow tracking. This is a direct extension and enhancement of traditional 2D segmentation. The method demonstrates quantitative performance with both over-segmentation and under-segmentation percentages around 5%, while achieving volume overlap exceeding 90% compared to expert manual segmentation, validated across synthesized and real 3D biological images, including Caenorhabditis elegans embryos and zebrafish nuclei. Subsequently, deep learning approaches U-Net (111) and its 3D variants (70, 68) have demonstrated exceptional performance in segmenting cellular populations and vascular networks within teravoxel brain volumetric images, achieving 3D IoU scores that exceed 85% for neuronal soma detection and 78% for vascular structure delineation (111, 95). Advanced attention mechanisms and transformer-based architectures have been integrated into these frameworks to capture long-range spatial dependencies that are particularly relevant to analyze distributed pathological patterns across entire brain hemispheres (112, 113). Recently, a work found that 3D cell segmentation extended directly from 2D is not robust for anisotropic resolution in whole brain LSFM (32). A novel 2D-to-3D manner is proposed with more robustness and efficiency. However, these 3D CV methodologies have not been scaled to a teravoxel whole-brain image.

The comprehensive 3D teravoxel analysis pipeline represents a shift from the extraction of RoI in 2D

(Fig. 2l) to whole brain profiling for statistical analysis (Fig. 2m), as intact tissue is imaged by LSFM rather than a brain section by BFM. Thus, the robustness of preprocessing and the high throughput of 3D CV algorithms are driving factors for trustworthy, efficient whole-brain profiling and consequent new neuropathological analysis. Although the entire cellular organization of cleared tissues can be rapidly imaged using LSFM at acquisition rates 2 to 3 orders of magnitude faster than point scanning systems (54, 55), day-long scanning in mammalian brains with large volume leads to challenging preprocessing of volumetric image stitching (Fig. 2e). The stitching problem is rooted in the fundamental trade-off between the limited size of the field of view (FOV) and the high resolution of microscopy. Achieving cellular-level detail across an entire mouse brain requires acquisition strategies by partitioning the imaging volume into manageable segments and slices. Consequently, challenging registration between 3D segments is represented by the various movements (ΔX vs. Z in Fig. 2e) across different slices due to the long scanning time.

3.3. 3D Reconstruction: Stitching

The earliest implementations of LSFM stitching relied heavily on manual alignment procedures, reflecting the limited computational infrastructure and algorithmic sophistication available during the initial development of light sheet microscopy systems. These pioneering approaches required extensive user intervention to specify correspondence points between overlapping image regions, typically employing simple translation models to achieve basic tile alignment. The computational demands of these early methods were substantial, often requiring days or weeks of processing time for even modest whole-brain datasets (114).

The TrakEM2 software package represented one of the first comprehensive and semi-automated solutions for large-scale image stitching (114). This system implemented manual registration capabilities that allowed researchers to specify correspondence points between adjacent tiles, applying rigid transformation models (115) to achieve initial alignment. The approach utilized interactive visualization tools to enable precise manual positioning of image tiles, although the process remained extremely time-intensive for large datasets.

Early automated approaches began to incorporate cross-correlation techniques to identify optimal alignment parameters between overlapping image regions (116). These methods computed normalized cross-correlation coefficients across predefined search windows, identifying translation offsets that maximized correlation between adjacent tiles. While representing a significant advancement over purely manual approaches, these early correlation-based methods struggled with illumination variations and geometric distortions characteristic of LSFM acquisitions (117, 118).

The introduction of phase correlation techniques (119) marked a significant advancement in LSFM stitching methodologies (120, 81), leveraging frequency domain representations to achieve more robust and efficient alignment. These approaches exploited the Fourier shift theorem to compute translation parameters directly from the phase information of overlapping image regions, providing improved accuracy and computational efficiency compared to spatial domain methods. Preibisch introduced the globally optimal stitching framework, implementing phase correlation for pairwise shift estimation coupled with global optimization algorithms to minimize accumulated registration errors (120). As a representative of the phase correlation-based method, this approach indicates another fundamental shift from sequential alignment procedures to global optimization strategies that consider the entire tile configuration simultaneously. The method demonstrated significant improvements in registration accuracy, particularly for large tile arrays where accumulated errors could become substantial. The Scale-Invariant Feature Transform (SIFT) algorithm (121), afterward, was integrated into the stitching pipelines, providing enhanced robustness to illumination variations and geometric distortions. Such hybrid approaches combined the computational efficiency of phase correlation with the geometric robustness of feature-based matching, allowing for more accurate alignment of tiles exhibiting significant photometric differences (115). The incorporation of SIFT features also facilitated the detection and correction of systematic geometric distortions inherent to LSFM

optical systems (122).

TeraStitcher (81), based on phase correlation, represents a significant advancement in high-performance computing solutions for large-scale LSFM stitching. The key innovation is the multi-level parallelization strategy, which exploits both thread-level and process-level parallelism, enabling efficient distribution of computational workload across multiple processing cores and nodes (123). This design significantly reduces processing time for large datasets while maintaining registration accuracy within 1-2 pixels for typical applications. The system utilized hierarchical data structures and optimized Input/Output (I/O) operations to achieve efficient processing of massive tile arrays while maintaining sub-pixel registration accuracy and minimal memory usage (<8GB).

Advanced stitching frameworks began to incorporate elastic registration techniques to account for tissue deformation and non-rigid distortions that occur during specimen preparation and imaging (124). The method implemented deformation models that could capture local tissue movements while maintaining global geometric coherence. This results in substantial computational resources along with significant improvements in registration accuracy for large and deformable specimens.

The BigStitcher platform represented a major advancement in scalable LSFM stitching, specifically designed to handle the massive datasets characteristic of whole brain imaging protocols (125). This system integrated advanced memory management strategies, distributed computing capabilities, and optimized algorithms to enable the processing of teravoxel-scale images (126). The platform implemented multiple registration algorithms, including phase correlation, Lucas-Kanade optimization, and interest point-based approaches, providing users with flexible options for interactive stitching.

The WobblyStitcher algorithm, integrated within the ClearMap2 software suite, introduced novel approaches for handling non-rigid deformations and geometric distortions commonly encountered in tissue clearing protocols (127). This method implemented advanced elastic registration techniques combined with robust outlier detection mechanisms to achieve accurate alignment of tiles exhibiting significant geometric variations (86). The algorithm demonstrated particular effectiveness in processing specimens that had undergone extensive tissue clearing procedures, where conventional rigid registration approaches often failed due to tissue deformation and optical distortions (128).

The modern ImarisStitcher system, developed by Bitplane, provided a comprehensive commercial solution for LSFM stitching with an emphasis on user-friendly interfaces and integrated visualization capabilities (129). This platform implemented multiple registration algorithms, including phase correlation, feature-based matching, and hybrid approaches, enabling users to select optimal methods based on the interactive ImarisViewer (130). The user-friendly graphic user interface (GUI) and the capability of dragging tile images in all dimensions facilitate user validation and refinement of stitching results.

3.4. Multiple Fluorescences: Colocalization

Modern LSFM systems can acquire volumetric images of entire mouse brains in hours, generating datasets containing billions of voxels in multiple fluorescence channels (131). The analysis of spatial relationships between different molecular markers within these teravoxel images requires efficient computing that can handle the unique challenges posed by cleared brain tissue imaging, including non-uniform signal distribution (132) and tissue deformation artifacts (133).

The foundation of quantitative colocalization analysis was established through the adaptation of Pearson's correlation coefficient (PCC) to confocal fluorescence microscopy prior to LSFM (134). This method evaluates the linear relationship between pixel intensities across two channels by calculating the correlation coefficient between the corresponding pixels in dual-channel images. The PCC approach was initially developed for confocal microscopy applications but was subsequently adapted for LSFM as the technology matured in the early 2000s (135). Despite its widespread adoption, PCC analysis demonstrated significant

limitations when applied to LSFM data, particularly in the presence of background fluorescence and when analyzing sparse cellular populations typical of whole-brain imaging. Building upon the PCC foundation, Mander's coefficients were developed to quantify the proportion of fluorescence in one channel that overlaps with fluorescence in a second channel (136). These coefficients address some limitations of PCC by providing asymmetric measures of colocalization, enabling researchers to determine whether marker A is contained within regions positive for marker B, and vice versa. The Manders coefficients became particularly relevant for LSFM applications where cellular markers might show different expression patterns or labeling efficiencies for the same cell across brain regions (54).

By standing on the shoulders of these foundation works, the evolution of colocalization methods for LSFM whole-brain imaging has progressed through distinct methodological phases over the past two decades. Before 2010, the cell colocalization between channels was intensity-based. The Intensity Correlation Analysis (ICA) method addressed the limitations of traditional correlation coefficients in distinguishing between dependent and independent fluorescence distributions (137). The ICA approach calculates the product of the differences from the mean (PDM) for each pixel pair, providing a more sensitive measure of pixel-wise correlation than traditional PCC methods. This technique proved particularly valuable for LSFM applications where weak colocalization signals might be masked by background fluorescence or where spatial heterogeneity in marker expression complicates analysis (138). The ICA method's ability to detect subtle correlations made it especially useful as an ImageJ plugin (139) for whole-brain LSFM. The automated thresholding approach objectively determines appropriate intensity thresholds for colocalization analysis without user bias (140). The method iteratively calculates PCC values for different threshold combinations and selects thresholds that maximize the correlation while maintaining statistical significance. This approach addressed a critical limitation in LSFM colocalization analysis, where manual threshold selection could introduce systematic bias across different brain regions or experimental conditions. The automated thresholding method became essential for processing large-scale LSFM datasets where manual threshold optimization for hundreds of brain regions would be impractical.

The 2010s witnessed the emergence of recognition-related methodologies, where traditional pixel-based methods could produce mistakes for objects of interest. They led to the development of object-based colocalization analysis approaches (141). These methods first segment individual cellular structures or molecular compounds for every channel, then the colocalization is produced between segmentation masks rather than pixel-wise intensities. This approach proved particularly valuable for LSFM applications in which cellular boundaries and subcellular structures can be clearly resolved (142). It reduces false positive cell colocalization that can arise from background fluorescence, since only objects of interest are segmented, and provides more neuroanatomy-related measures of spatial association between cellular objects. Building on object-based segmentation, distance-based colocalization methods quantify the spatial separation between identified objects to determine whether they are truly colocalized or merely adjacent (143). These approaches calculate minimum distances between object boundaries and apply statistical tests to determine whether observed distances are significantly different from random distributions. The distance-based analysis became crucial for LSFM applications where the high resolution might cause distinct but adjacent structures within the same cell to appear colocalized (144). The method's ability to account for the 3D nature of LSFM data made it particularly well-suited for whole-brain analysis where cellular structures extend across multiple Z-planes.

Afterward, the development of standardized brain atlases, particularly the Allen Common Coordinate Framework version 3 (CCFv3), enabled systematic registration of LSFM datasets in common reference spaces (85). A branch of studies (145, 146) reformulated the colocalization as a registration problem of aligning multichannel LSFM images to a common space of the annotated brain atlas. The method addresses challenges specific to LSFM imaging, including tissue deformation artifacts introduced by clearing

procedures and non-uniform signal distribution across multiple channels (147). Atlas registration not only advanced cell colocalization, but it also became essential for comparative studies and meta-analyzes of whole-brain LSFM datasets, providing standardized coordinate systems for quantifying spatial relationships between molecular markers, since it has been involved in the teravoxel analysis pipeline (Fig. 2m).

Deep learning-based colocalizations, such as (148, 149), provide supervised learning solutions for the common problem of diverse SNR among different channels of LSFM based on a convolutional long short-term memory (LSTM) neural network. The adaptive nature of these algorithms enables more robust analysis across different tissue-clearing methods, imaging conditions, and marker combinations, leading to teravoxel analysis of multiple cell types.

4. EMERGING APPLICATIONS OF TERAVOXEL MICROSCOPY IMAGE ANALYSIS FOR NEUROLOGY

The most recent applications of teravoxel microscopy image analysis for neurological diseases focus on the whole mouse brain vascular and neuronal system. Various SOTA teravoxel analysis pipelines in related studies were framed similarly as in Fig. 2m after the teravoxel image reconstruction. Different concerns have been explored on the feasibility of AI methodologies (150), the special properties of LSFM (such as anisotropic resolution (31)), and the efficiency of teravoxel computation (30). Considering this, the differences between applications can be summarized as predictive methodologies, objects of interest, and result reconstructions. Every application is a computing stream of small local patches fed into a local operator, which is illustrated in the workflow: (i) Reconstructing teravoxel input (Fig. 3a), (ii) two computation categories for every local patch (Fig. 3cd), and (iii) the whole-brain statistics for the neurological outcome based on whole-brain profiles at the cellular level (Fig. 3efgh).

3D Neural Network (NN) pipeline (Fig. 3c) and 2D NN pipeline (Fig. 3d) have demonstrated shared objectives and diverse computational efficiency (Fig. 3b). The 3D NN pipeline incorporates advanced methodologies spanning from watershed-based segmentation techniques (151) through 3D CNN (152) to the 3D Vision Transformer (ViT) architectures (153), demonstrating whole-brain profiling by vessel segmentation (25), and voxel-wise (69, 150) and patch-wise (154) nuclei classification tasks. In contrast, the 2D pipeline leverages U-Net architectures (111) and a hybrid 2D CNN + GNN framework (32) for efficient nuclei detection and colocalization (30), and instance segmentation (32) across volumetric datasets. These state-of-the-art teravoxel microscopy image analysis applications are reviewed in this section regarding their pros and cons using a 3D or 2D pipeline.

4.1. 3D NN based Pipeline

The development of 3D NN architectures has fundamentally extended patch-based 3D CV methodologies to teravoxel image analysis, enabling direct tera-level voxel-wise prediction of cellular and vascular structure (Fig. 3eg). Early watershed-based segmentation approaches provided automated quantitative analysis of dense objects, establishing an earlier framework that detects nuclei in the whole mouse brain (150). Multiple Cre mice were used for cell segmenting and counting in each region, as well as fiber tract segmentation, to map the rabies-EGFP process in the whole mouse brain.

The 3D U-net was also scaled up to teravoxel, indicating a significant advancement in computational efficiency and analytical precision. (25) developed a machine learning framework specifically designed for whole mouse brain vasculature mapping (vessel map in Fig. 3e), demonstrating how 3D CNN architectures could effectively capture complex vessel morphologies and network topologies across teravoxel datasets. The reported evidence of secondary intracranial collateral vascularization in CD1 mice (longer vessel length in Fig. 3e) and reduced vascularization of the brainstem in comparison to the cerebrum revealed unbiased and

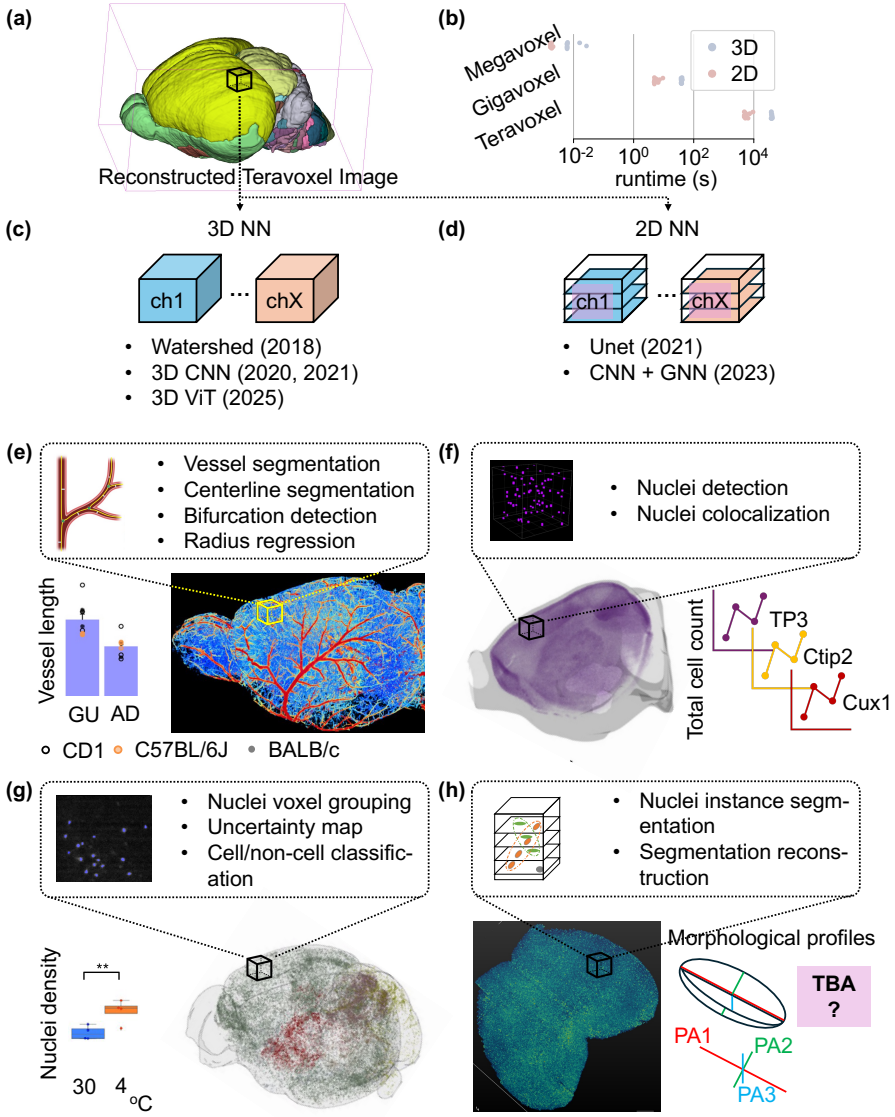

Figure 3

Existing applications of teravoxel image analysis can be categorized into two types, 3D and 2D approaches, after (a) the whole-brain image is reconstructed (tile stitching and channel alignment between ch1 to chX). They are differentiated by 3D and 2D operators, respectively, resulting in (b) runtimes of 2D approaches are consistently faster than 3D, with lower than 10^4 seconds for teravoxel whole-brain images. (c) 3D operators in existing applications include watershed (150), 3D CNN (25, 154), and 3D ViT (69) for (e) vessel segmentation (25) and (g) nuclei voxel grouping (69) from volumetric inputs, where vessel and nuclei plots are adapted from corresponding literature, respectively. On the other hand, (d) 2D operators include Unet, CNN, and GNN, (f) predict nuclei locations (30) and (h) reconstruct instance segmentation (32) in 3D from 2D patches, respectively, where cell count and morphology plots are adapted from corresponding literature. Although whole-brain studies differ from computational approaches, the whole-brain profiles of 3D cellular biomarkers brought novel associations between (e) vessel length and brain region (GU: Gustatory areas; AD: Anterodorsal nucleus), (f) counting across different cell types (TP3: TO-PRO-3), (g) nuclei density and temperature of exposure, and (h) a to-be-announced (TBA) whole-brain profile of nuclei Principal Axis (PA).

scalable quantifications of the angioarchitecture of the mouse brain. This work established critical precedents for automated vascular phenotyping and enabled systematic quantification of vascular parameters that were previously inaccessible through conventional analysis methods.

Subsequent developments in deep learning methodologies further enhanced the precision of cellular detection and segmentation capabilities. (154) introduced specialized algorithms for 3D cell detection in whole mouse brain datasets, achieving >95% accuracy in local patch classification, whether there is a cell, across various brain regions. Unlike voxel-wise prediction in previous works, patch-based ($50\times50\times20\mu m^3$) classification leads to high efficiency (91 mins/brain) with coarse cell detection. Their efficient pipeline demonstrated that the algorithm cell counts are correlated with manual cell counts (>0.99) for large-scale cellular phenotyping.

The utilization of 3D ViT architectures in 2025 represents the latest evolution in this teravoxel analysis trajectory, offering an artificial intelligence-based cartography of ensembles (ACE) pipeline by enhanced attention mechanisms (69). It enabled unbiased mapping of local neuronal activity and connectivity. It demonstrated superior segmentation accuracy, advanced by uncertainty mapping and Monte Carlo dropout. The statistical analysis between mice acclimated in different temperatures quantitatively measured c-Fos immunolabeled cells (nuclei density in Fig. 3g) under different environmental stimuli.

4.2. 2D NN based Pipeline

The 2D CNN is more efficient than the 3D CNN as exemplified in Fig. 3b since it uses 2D filters. The computation of data with a teravoxel scale can be done in hours by 2D methods, while 3D methods can take days. Therefore, several recent studies have a 2D-to-3D methodology in their pipeline to increase efficiency (30) and to address anisotropic resolution as well (32).

The differences in the 2D pipeline (Fig. 3d) are (i) computing 2D slices with higher resolution, and (ii) reconstructing 2D results to 3D along the low-resolution axis. NuMorph (30) was proposed to predict nuclei as dots (nuclei cloud in Fig. 3f) for cell counting across multiple fluorescence channels. Based on a threshold-based colocalization algorithm, total cell counts and spatial correlation among different stained cell types are statistically compared between wild-type mice and gene-modified mice, demonstrating quantitative results of neuron overgrowth since the cell counts in the isocortex region of gene-modified mice are increasing.

The anisotropic resolution was reported as a defect for 3D volumetric segmentation (32), causing inaccurate (<80%) instance segmentation by 3D CNN. 2D CNN was used in this work, incorporated with a GNN-based 2D-to-3D approach to group the 2D segmentation masks as a complete 3D prediction. This attempt first presents whole-brain instance segmentation, enabling cellular morphology mapping in teravoxel image analysis (nuclei volume map in Fig. 3h).

4.3. Future Directions

4.3.1. Cell Morphology Whole-Brain Profiling The development of morphological characterization of cells and neurons represents a fundamental advancement in quantitative neuroanatomy. Current analytical pipelines primarily focus on basic geometric parameters such as location, density, and size measurements of cells and vessels, yet the complex 3D morphology of nuclear and neuron populations demands more approaches. As 3D robust nuclei instance segmentation demonstrated in whole brain LSFM (32), future computational frameworks could integrate advanced shape descriptors, including spherical harmonic decomposition (155), and principal axis measures (morphological profiles in Fig. 3h) to capture nuanced morphological variations that characterize different cellular phenotypes and pathological states.

4.3.2. Error-Resistant Teravoxel Image Analysis Pipeline Although statistical results as new biomarkers, e.g., vascular measurements (25), provided new neurological insights for brain disorder early diagnosis, complex preprocessing steps (Fig. 2ek) can cause errors accumulated in statistical results. Since 3D and 2D-based pipelines consume most of the time for computation after teravoxel image preprocessing (10^4 seconds in Fig. 3b), the redo of data analysis will double the time cost to correct preprocessing errors, where small errors in teravoxel-scale data are hard to find yet fatal for the conclusion. An error-resistant pipeline can be formed by (i) analyzing raw data before the reconstruction of teravoxel volumetric image, and (ii) calculating the transformation parameters of raw data, which can be applied later on to analytical results as needed.

4.3.3. Cellular Pathology and Morphology Coupling An investigation (156) represented an innovative multimodal platform integrating LSFM with 18F-flutemetamol PET and MRI to establish quantitative 3D correlations between β-amyloid pathology in ocular and cerebral tissues. Although the proposed method reconstructed Aβ, microglia, and astrocytes from LSFM to a 3D surface instead of a teravoxel image, this study demonstrated a significant difference (p <0.001) between the amyloid plaque surface volume of AD and control groups. The PET standardized uptake value ratios (SUVRs) with weaker statistics, non-significant between AD and control (p =0.167), established the first quantitative evidence of multimodal analysis of pathological and morphological features in cellular resolution across the whole brain surface. This potential proved that emerging longitudinal multimodal studies for coupling cellular pathology and morphology can further advance our understanding of neurological diseases with the gold standard datasets.

These improvements will allow us to better understand neurological disease processes. They will link cellular pathology with systems-level phenotypes, which have long hindered our understanding of complex neurobiological disorders.

5. CONCLUSIONS

The emergence of light sheet fluorescence microscopy (LSFM) coupled with artificial intelligence-driven analysis represents a paradigm-shifting transformation in neurological disease research, fundamentally surpassing the resolution and specificity limitations inherent to non-invasive neuroimaging modalities. This convergence has enabled unprecedented access to cellular-level structural details in intact brain tissue, generating a teravoxel image that captures neuronal morphology, vascular networks, and pathological protein distributions with subcellular precision. The evolution from gigapixel whole-slide imaging to comprehensive 3D volumetric analysis has necessitated efficient and robust computational frameworks capable of preprocessing, detecting, and segmenting objects of interest, where the data scale exceeds non-invasive neuroimaging by several orders of magnitude.

Teravoxel analysis pipelines have demonstrated both 3D and 2D neural network-based methodologies, each offering distinct computational trade-offs between precision and efficiency. The implementation of advanced deep learning methodologies, ranging from 3D U-Net, ViT architectures for vascular mapping, to hybrid 2D CNN-GNN frameworks for nuclei instance segmentation, has enabled systematic characterization of cellular populations and morphological alterations previously inaccessible through non-invasive neuroimaging. These computational advances have yielded quantitative insights into neuroinflammatory responses, neurodegenerative processes, and vascular pathology. Simultaneously, unique challenges of LSFM, including non-rigid stitching and multichannel fluorescence, are considered. Methodological standards are established for investigating neurological disease mechanisms at the cellular scale across the whole brain, quantitatively.

DISCLOSURE STATEMENT

The authors are not aware of any affiliations, memberships, funding, or financial holdings that might be perceived as affecting the objectivity of this review.

LITERATURE CITED

1. Moura MC, Casulari LA, Novaes MRCG. 2016. A predictive model for prognosis in motor neuron disease. *Journal of neurological disorders* 4(8)
2. Westeneng HJ, Debray TP, Visser AE, van Eijk RP, Rooney JP, et al. 2018. Prognosis for patients with amyotrophic lateral sclerosis: development and validation of a personalised prediction model. *The Lancet Neurology* 17(5):423–433
3. Kotsavasiloglou C, Kostikis N, Hristu-Varsakelis D, Arnaoutoglou M. 2017. Machine learning-based classification of simple drawing movements in Parkinson's disease. *Biomedical Signal Processing and Control* 31:174–180
4. Zhang B, Gaiteri C, Bodea LG, Wang Z, McElwee J, et al. 2013. Integrated systems approach identifies genetic nodes and networks in late-onset Alzheimer's disease. *Cell* 153(3):707–720
5. Myszczynska MA, Ojamies PN, Lacoste AM, Neil D, Saffari A, et al. 2020. Applications of machine learning to diagnosis and treatment of neurodegenerative diseases. *Nature reviews neurology* 16(8):440–456
6. Sharma VK, Singh TG, Mehta V, Mannan A. 2023. Biomarkers: Role and scope in neurological disorders. *Neurochemical Research* 48(7):2029–2058
7. Bennett RE, Robbins AB, Hu M, Cao X, Betensky RA, et al. 2018. Tau induces blood vessel abnormalities and angiogenesis-related gene expression in P301L transgenic mice and human Alzheimer's disease. *Proceedings of the National Academy of Sciences* 115(6):E1289–E1298
8. Jack Jr CR, Bernstein MA, Fox NC, Thompson P, Alexander G, et al. 2008. The Alzheimer's disease neuroimaging initiative (ADNI): MRI methods. *Journal of Magnetic Resonance Imaging: An Official Journal of the International Society for Magnetic Resonance in Medicine* 27(4):685–691
9. Marcus DS, Wang TH, Parker J, Csernansky JG, Morris JC, Buckner RL. 2007. Open Access Series of Imaging Studies (OASIS): cross-sectional MRI data in young, middle aged, nondemented, and demented older adults. *Journal of cognitive neuroscience* 19(9):1498–1507
10. Sudlow C, Gallacher J, Allen N, Beral V, Burton P, et al. 2015. UK biobank: an open access resource for identifying the causes of a wide range of complex diseases of middle and old age. *PLoS medicine* 12(3):e1001779
11. Allen EJ, St-Yves G, Wu Y, Breedlove JL, Prince JS, et al. 2022. A massive 7T fMRI dataset to bridge cognitive neuroscience and artificial intelligence. *Nature neuroscience* 25(1):116–126
12. Fischl B. 2012. FreeSurfer. *Neuroimage* 62(2):774–781
13. Jenkinson M, Beckmann CF, Behrens TE, Woolrich MW, Smith SM. 2012. Fsl. *Neuroimage* 62(2):782–790
14. Caro JO, Fonseca AHdO, Averill C, Rizvi SA, Rosati M, et al. 2023. Brainlm: A foundation model for brain activity recordings. *bioRxiv* :2023–09
15. Yang Y, Ye C, Su G, Zhang Z, Chang Z, et al. 2024. Brainmass: Advancing brain network analysis for diagnosis with large-scale self-supervised learning. *IEEE Transactions on Medical Imaging*
16. Wei Z, Dan T, Ding J, Laurienti P, Wu G. 2024. *Representing Functional Connectivity with Structural Detour: A New Perspective to Decipher Structure-Function Coupling Mechanism*. In *International Conference on Medical Image Computing and Computer-Assisted Intervention*, pp. 367–377. Springer
17. Wei Z, Dan T, Ding J, Wu G. 2024. NeuroPath: A neural pathway transformer for joining the dots of human connectomes. *Advances in Neural Information Processing Systems* 37:67826–67849
18. Dournaud P, Gu YZ, Schonbrunn A, Mazella J, Tannenbaum GS, Beaudet A. 1996. Localization of the somatostatin receptor SST2A in rat brain using a specific anti-peptide antibody. *Journal of Neuroscience* 16(14):4468–4478
19. Weinstein JN, Collisson EA, Mills GB, Shaw KR, Ozenberger BA, et al. 2013. The cancer genome atlas pan-cancer analysis project. *Nature genetics* 45(10):1113–1120
20. Siedentopf H, Zsigmondy R. 1902. Uber sichtbarmachung und größenbestimmung ultramikoskopischer teilchen, mit besonderer anwendung auf goldrubingläser. *Annalen der Physik* 315(1):1–39

21. Spalteholz W. 1911. *Über das Durchsightigmachen von menschlichen und tierischen Präparaten: nebst Anhang, Über Knochenfärbung*. S. Hirzel
22. Voie AH, Burns D, Spelman F. 1993. Orthogonal-plane fluorescence optical sectioning: Three-dimensional imaging of macroscopic biological specimens. *Journal of microscopy* 170(3):229–236
23. Dodt HU, Leischner U, Schierloh A, Jährling N, Mauch CP, et al. 2007. Ultramicroscopy: three-dimensional visualization of neuronal networks in the whole mouse brain. *Nature methods* 4(4):331–336
24. Gornet J, Venkataraju KU, Narasimhan A, Turner N, Lee K, et al. 2019. *Reconstructing neuronal anatomy from whole-brain images*. In *2019 IEEE 16th International Symposium on Biomedical Imaging (ISBI 2019)*, pp. 218–222. IEEE
25. Todorov MI, Paetzold JC, Schoppe O, Tetteh G, Shit S, et al. 2020. Machine learning analysis of whole mouse brain vasculature. *Nature methods* 17(4):442–449
26. Ueda HR, Dodt HU, Osten P, Economo MN, Chandrashekar J, Keller PJ. 2020. Whole-brain profiling of cells and circuits in mammals by tissue clearing and light-sheet microscopy. *Neuron* 106(3):369–387
27. Schubert PJ, Dorkenwald S, Januszewski M, Klimesch J, Svara F, et al. 2022. SyConn2: dense synaptic connectivity inference for volume electron microscopy. *Nature Methods* 19(11):1367–1370
28. Coronado-Leija R, Abdollahzadeh A, Lee HH, Coelho S, Ades-Aron B, et al. 2024. Volume electron microscopy in injured rat brain validates white matter microstructure metrics from diffusion mri. *Imaging Neuroscience* 2:1–20
29. Lin S, Sprague T, Singh AK. 2022. Mind reader: Reconstructing complex images from brain activities. *Advances in Neural Information Processing Systems* 35:29624–29636
30. Krupa O, Fragola G, Hadden-Ford E, Mory JT, Liu T, et al. 2021. NuMorph: Tools for cortical cellular phenotyping in tissue-cleared whole-brain images. *Cell reports* 37(2)
31. Wei Z, Dan T, Ding J, McCormick C, Kyere FA, et al. 2023. *High Throughput Deep Model of 3D Nucleus Instance Segmentation by Stereo Stitching Contextual Gaps*. In *2023 IEEE 20th International Symposium on Biomedical Imaging (ISBI)*, pp. 1–5. IEEE
32. Wei Z, Dan T, Ding J, Dere M, Wu G. 2023. *A General Stitching Solution for Whole-Brain 3D Nuclei Instance Segmentation from Microscopy Images*. In *International Conference on Medical Image Computing and Computer-Assisted Intervention*, pp. 46–55. Springer
33. Goerner FL, Clarke GD. 2011. Measuring signal-to-noise ratio in partially parallel imaging mri. *Medical physics* 38(9):5049–5057
34. Yan J, Schaefferkoetter J, Conti M, Townsend D. 2016. A method to assess image quality for low-dose pet: analysis of snr, cnr, bias and image noise. *Cancer Imaging* 16(1):26
35. Judy PF, Swensson RG, Szulc M. 1981. Lesion detection and signal–to–noise ratio in ct images. *Medical physics* 8(1):13–23
36. Foylan S, Rooney L, Amos W, Gould G, McConnell G. 2025. PerfectlyAverage: A classical open-source software method to determine the optimal averaging parameters in laser scanning fluorescence microscopy. *Journal of Microscopy*
37. Glasser MF, Sotiropoulos SN, Wilson JA, Coalson TS, Fischl B, et al. 2013. The minimal preprocessing pipelines for the human connectome project. *Neuroimage* 80:105–124
38. Poldrack RA, Baker CI, Durnez J, Gorgolewski KJ, Matthews PM, et al. 2017. Scanning the horizon: towards transparent and reproducible neuroimaging research. *Nature reviews neuroscience* 18(2):115–126
39. Van Essen DC, Smith SM, Barch DM, Behrens TE, Yacoub E, et al. 2013. The wu-minn human connectome project: an overview. *Neuroimage* 80:62–79
40. Brown C, Das S, Xie L, Nasrallah I, Detre J, et al. 2024. Medial temporal lobe gray matter microstructure in preclinical Alzheimer's disease. *Alzheimer's & Dementia* 20(6):4147–4158
41. Ren J, An N, Lin C, Zhang Y, Sun Z, et al. 2025. DeepPrep: an accelerated, scalable and robust pipeline for neuroimaging preprocessing empowered by deep learning. *Nature Methods* :1–4
42. Roland P, Graufelds C, Wählin J, Ingelman L, Andersson M, et al. 1994. Human brain atlas: for high-resolution functional and anatomical mapping. *Human brain mapping* 1(3):173–184
43. Fotiadis P, Parkes L, Davis KA, Satterthwaite TD, Shinohara RT, Bassett DS. 2024. Structure–function coupling

in macroscale human brain networks. *Nature Reviews Neuroscience* 25(10):688–704
44. Liu S, Liu S, Cai W, Che H, Pujol S, et al. 2014. Multimodal neuroimaging feature learning for multiclass diagnosis of Alzheimer's disease. *IEEE transactions on biomedical engineering* 62(4):1132–1140
45. Ktena SI, Parisot S, Ferrante E, Rajchl M, Lee M, et al. 2017. *Distance metric learning using graph convolutional networks: Application to functional brain networks*. In *Medical Image Computing and Computer Assisted Intervention- MICCAI 2017: 20th International Conference, Quebec City, QC, Canada, September 11-13, 2017, Proceedings, Part I 20*, pp. 469–477. Springer
46. Ding J, Dan T, Wei Z, Cho H, Laurienti PJ, et al. 2024. Machine learning on dynamic functional connectivity: Promise, pitfalls, and interpretations. *arXiv preprint arXiv:2409.11377*
47. Muganga T, Sasse L, Larabi DI, Nieto N, Caspers J, et al. 2025. Voxel-wise or region-wise nuisance regression for functional connectivity analyses: Does it matter? *Human brain mapping* 46(12):e70323
48. Bullmore E, Sporns O. 2009. Complex brain networks: graph theoretical analysis of structural and functional systems. *Nature reviews neuroscience* 10(3):186–198
49. Ktena SI, Parisot S, Ferrante E, Rajchl M, Lee M, et al. 2018. Metric learning with spectral graph convolutions on brain connectivity networks. *NeuroImage* 169:431–442
50. Yao D, Sui J, Wang M, Yang E, Jiaerken Y, et al. 2021. A mutual multi-scale triplet graph convolutional network for classification of brain disorders using functional or structural connectivity. *IEEE transactions on medical imaging* 40(4):1279–1289
51. Plis SM, Hjelm DR, Salakhutdinov R, Allen EA, Bockholt HJ, et al. 2014. Deep learning for neuroimaging: a validation study. *Frontiers in neuroscience* 8:229
52. Yang B, Lange M, Millett-Sikking A, Zhao X, Bragantini J, et al. 2022. Daxi—high-resolution, large imaging volume and multi-view single-objective light-sheet microscopy. *Nature methods* 19(4):461–469
53. Keller PJ, Schmidt AD, Wittbrodt J, Stelzer EH. 2008. Reconstruction of zebrafish early embryonic development by scanned light sheet microscopy. *science* 322(5904):1065–1069
54. Richardson DS, Lichtman JW. 2015. Clarifying tissue clearing. *Cell* 162(2):246–257
55. Ueda HR, Ertürk A, Chung K, Gradinaru V, Chédotal A, et al. 2020. Tissue clearing and its applications in neuroscience. *Nature Reviews Neuroscience* 21(2):61–79
56. Swoger J, Verveer P, Greger K, Huisken J, Stelzer EH. 2007. Multi-view image fusion improves resolution in three-dimensional microscopy. *Optics express* 15(13):8029–8042
57. Dean KM, Roudot P, Welf ES, Danuser G, Fiolka R. 2015. Deconvolution-free subcellular imaging with axially swept light sheet microscopy. *Biophysical journal* 108(12):2807–2815
58. Hillman EM, Voleti V, Li W, Yu H. 2019. Light-sheet microscopy in neuroscience. *Annual review of neuroscience* 42(1):295–313
59. Renier N, Wu Z, Simon DJ, Yang J, Ariel P, Tessier-Lavigne M. 2014. iDISCO: a simple, rapid method to immunolabel large tissue samples for volume imaging. *Cell* 159(4):896–910
60. Gu S, Ran C. 2025. Advanced optical microscopic imaging techniques for imaging amyloid beta and deciphering Alzheimer's disease pathogenesis. *Iradiology* 3(2):95–114
61. Pham C, Moro DH, Mouffle C, Didienne S, Hepp R, et al. 2020. Mapping astrocyte activity domains by light sheet imaging and spatio-temporal correlation screening. *Neuroimage* 220:117069
62. Liebmann T, Renier N, Bettayeb K, Greengard P, Tessier-Lavigne M, Flajolet M. 2016. Three-dimensional study of Alzheimer's disease hallmarks using the idisco clearing method. *Cell reports* 16(4):1138–1152
63. Morawski M, Kirilina E, Scherf N, Jäger C, Reimann K, et al. 2018. Developing 3d microscopy with clarity on human brain tissue: Towards a tool for informing and validating mri-based histology. *Neuroimage* 182:417–428
64. Chen BC, Legant WR, Wang K, Shao L, Milkie DE, et al. 2014. Lattice light-sheet microscopy: imaging molecules to embryos at high spatiotemporal resolution. *Science* 346(6208):1257998
65. Stelzer EH. 2015. Light-sheet fluorescence microscopy for quantitative biology. *Nature methods* 12(1):23–26
66. Goedert M, Spillantini MG. 2006. A century of Alzheimer's disease. *science* 314(5800):777–781
67. Spires-Jones TL, Hyman BT. 2014. The intersection of amyloid beta and tau at synapses in Alzheimer's disease. *Neuron* 82(4):756–771
68. Yin J, Yang G, Qin X, Li H, Wang L. 2022. Optimized u-net model for 3d light-sheet image segmentation of

zebrafish trunk vessels. *Biomedical Optics Express* 13(5):2896–2908
69. Attarpour A, Osmann J, Rinaldi A, Qi T, Lal N, et al. 2025. A deep learning pipeline for three-dimensional brain-wide mapping of local neuronal ensembles in teravoxel light-sheet microscopy. *Nature methods* :1–12
70. Çiçek Ö, Abdulkadir A, Lienkamp SS, Brox T, Ronneberger O. 2016. *3D U-Net: learning dense volumetric segmentation from sparse annotation*. In *Medical Image Computing and Computer-Assisted Intervention–MICCAI 2016: 19th International Conference, Athens, Greece, October 17-21, 2016, Proceedings, Part II 19*, pp. 424–432. Springer
71. Moen E, Bannon D, Kudo T, Graf W, Covert M, Van Valen D. 2019. Deep learning for cellular image analysis. *Nature methods* 16(12):1233–1246
72. Peng H, Hawrylycz M, Roskams J, Hill S, Spruston N, et al. 2015. BigNeuron: large-scale 3d neuron reconstruction from optical microscopy images. *Neuron* 87(2):252–256
73. Zhou Z, Kuo HC, Peng H, Long F. 2018. DeepNeuron: an open deep learning toolbox for neuron tracing. *Brain informatics* 5:1–9
74. Januszewski M, Kornfeld J, Li PH, Pope A, Blakely T, et al. 2018. High-precision automated reconstruction of neurons with flood-filling networks. *Nature methods* 15(8):605–610
75. Cai Y, Zhang X, Li C, Ghashghaei HT, Greenbaum A. 2023. COMBINe enables automated detection and classification of neurons and astrocytes in tissue-cleared mouse brains. *Cell Reports Methods* 3(4)
76. Berg S, Kutra D, Kroeger T, Straehle CN, Kausler BX, et al. 2019. Ilastik: interactive machine learning for (bio) image analysis. *Nature methods* 16(12):1226–1232
77. Borland D, McCormick CM, Patel NK, Krupa O, Mory JT, et al. 2021. Segmentor: a tool for manual refinement of 3d microscopy annotations. *BMC bioinformatics* 22(1):260
78. Chen T, Kornblith S, Norouzi M, Hinton G. 2020. *A simple framework for contrastive learning of visual representations*. In *International conference on machine learning*, pp. 1597–1607. PmLR
79. He K, Chen X, Xie S, Li Y, Dollár P, Girshick R. 2022. *Masked autoencoders are scalable vision learners*. In *Proceedings of the IEEE/CVF conference on computer vision and pattern recognition*, pp. 16000–16009
80. Newmaster KT, Kronman FA, Wu Yt, Kim Y. 2022. Seeing the forest and its trees together: implementing 3d light microscopy pipelines for cell type mapping in the mouse brain. *Frontiers in neuroanatomy* 15:787601
81. Bria A, Iannello G. 2012. TeraStitcher-a tool for fast automatic 3d-stitching of teravoxel-sized microscopy images. *BMC bioinformatics* 13:1–15
82. Gautier MK, Ginsberg SD. 2021. A method for quantification of vesicular compartments within cells using 3d reconstructed confocal z-stacks: comparison of imagej and imaris to count early endosomes within basal forebrain cholinergic neurons. *Journal of neuroscience methods* 350:109038
83. Susaki EA, Tainaka K, Perrin D, Yukinaga H, Kuno A, Ueda HR. 2015. Advanced cubic protocols for whole-brain and whole-body clearing and imaging. *Nature protocols* 10(11):1709–1727
84. Tomer R, Ye L, Hsueh B, Deisseroth K. 2014. Advanced clarity for rapid and high-resolution imaging of intact tissues. *Nature protocols* 9(7):1682–1697
85. Wang Q, Ding SL, Li Y, Royall J, Feng D, et al. 2020. The allen mouse brain common coordinate framework: a 3d reference atlas. *Cell* 181(4):936–953
86. Kirst C, Skriabine S, Vieites-Prado A, Topilko T, Bertin P, et al. 2020. Mapping the fine-scale organization and plasticity of the brain vasculature. *Cell* 180(4):780–795
87. Gurcan MN, Boucheron LE, Can A, Madabhushi A, Rajpoot NM, Yener B. 2009. Histopathological image analysis: A review. *IEEE reviews in biomedical engineering* 2:147–171
88. Madabhushi A, Lee G. 2016. Image analysis and machine learning in digital pathology: Challenges and opportunities. *Medical image analysis* 33:170–175
89. Fuchs TJ, Wild PJ, Moch H, Buhmann JM. 2008. *Computational pathology analysis of tissue microarrays predicts survival of renal clear cell carcinoma patients*. In *International Conference on Medical Image Computing and Computer-Assisted Intervention*, pp. 1–8. Springer
90. Das K, Conjeti S, Roy AG, Chatterjee J, Sheet D. 2018. *Multiple instance learning of deep convolutional neural networks for breast histopathology whole slide classification*. In *2018 IEEE 15th International Symposium on Biomedical Imaging (ISBI 2018)*, pp. 578–581. IEEE

91. Sari CT, Gunduz-Demir C. 2018. Unsupervised feature extraction via deep learning for histopathological classification of colon tissue images. *IEEE transactions on medical imaging* 38(5):1139–1149
92. Jafari-Khouzani K, Soltanian-Zadeh H. 2003. Multiwavelet grading of pathological images of prostate. *IEEE Transactions on Biomedical Engineering* 50(6):697–704
93. Basavanhally A, Ganesan S, Feldman M, Shih N, Mies C, et al. 2013. Multi-field-of-view framework for distinguishing tumor grade in er+ breast cancer from entire histopathology slides. *IEEE transactions on biomedical engineering* 60(8):2089–2099
94. Cruz-Roa A, Gilmore H, Basavanhally A, Feldman M, Ganesan S, et al. 2017. Accurate and reproducible invasive breast cancer detection in whole-slide images: A deep learning approach for quantifying tumor extent. *Scientific reports* 7(1):46450
95. Falk T, Mai D, Bensch R, Çiçek Ö, Abdulkadir A, et al. 2019. U-Net: deep learning for cell counting, detection, and morphometry. *Nature methods* 16(1):67–70
96. Hou L, Samaras D, Kurc TM, Gao Y, Davis JE, Saltz JH. 2016. *Patch-based convolutional neural network for whole slide tissue image classification.* In *Proceedings of the IEEE conference on computer vision and pattern recognition*, pp. 2424–2433
97. Hamilton PW, Bankhead P, Wang Y, Hutchinson R, Kieran D, et al. 2014. Digital pathology and image analysis in tissue biomarker research. *Methods* 70(1):59–73
98. Janowczyk A, Madabhushi A. 2016. Deep learning for digital pathology image analysis: A comprehensive tutorial with selected use cases. *Journal of pathology informatics* 7(1):29
99. Wang D, Khosla A, Gargeya R, Irshad H, Beck AH. 2016. Deep learning for identifying metastatic breast cancer. *arXiv preprint arXiv:1606.05718*
100. Lee CS, Latimer CS, Henriksen JC, Blazes M, Larson EB, et al. 2021. Application of deep learning to understand resilience to Alzheimer's disease pathology. *Brain Pathology* 31(6):e12974
101. He K, Zhang X, Ren S, Sun J. 2016. *Deep residual learning for image recognition.* In *Proceedings of the IEEE conference on computer vision and pattern recognition*, pp. 770–778
102. Zhao H, Shi J, Qi X, Wang X, Jia J. 2017. *Pyramid scene parsing network.* In *Proceedings of the IEEE conference on computer vision and pattern recognition*, pp. 2881–2890
103. Signaevsky M, Prastawa M, Farrell K, Tabish N, Baldwin E, et al. 2019. Artificial intelligence in neuropathology: deep learning-based assessment of tauopathy. *Laboratory Investigation* 99(7):1019–1029
104. Kim M, Sekiya H, Yao G, Martin NB, Castanedes-Casey M, et al. 2023. Diagnosis of Alzheimer disease and tauopathies on whole-slide histopathology images using a weakly supervised deep learning algorithm. *Laboratory investigation* 103(6):100127
105. Tellez D, Litjens G, Van der Laak J, Ciompi F. 2019. Neural image compression for gigapixel histopathology image analysis. *IEEE transactions on pattern analysis and machine intelligence* 43(2):567–578
106. Faust K, Lee MK, Dent A, Fiala C, Portante A, et al. 2022. Integrating morphologic and molecular histopathological features through whole slide image registration and deep learning. *Neuro-Oncology Advances* 4(1):vdac001
107. Braak H, Braak E. 1991. Neuropathological stageing of Alzheimer-related changes. *Acta neuropathologica* 82(4):239–259
108. Schmied C, Steinbach P, Pietzsch T, Preibisch S, Tomancak P. 2016. An automated workflow for parallel processing of large multiview spim recordings. *Bioinformatics* 32(7):1112–1114
109. Ruan X, Mueller M, Liu G, Görlitz F, Fu TM, et al. 2024. Image processing tools for petabyte-scale light sheet microscopy data. *Nature Methods* :1–11
110. Li G, Liu T, Tarokh A, Nie J, Guo L, et al. 2007. 3D cell nuclei segmentation based on gradient flow tracking. *BMC cell biology* 8:1–10
111. Ronneberger O, Fischer P, Brox T. 2015. *U-Net: Convolutional networks for biomedical image segmentation.* In *Medical image computing and computer-assisted intervention–MICCAI 2015: 18th international conference, Munich, Germany, October 5-9, 2015, proceedings, part III 18*, pp. 234–241. Springer
112. Vaswani A, Shazeer N, Parmar N, Uszkoreit J, Jones L, et al. 2017. Attention is all you need. *Advances in neural information processing systems* 30

113. He K, Gan C, Li Z, Rekik I, Yin Z, et al. 2023. Transformers in medical image analysis. *Intelligent Medicine* 3(1):59–78
114. Cardona A, Saalfeld S, Schindelin J, Arganda-Carreras I, Preibisch S, et al. 2012. TrakEM2 software for neural circuit reconstruction. *PloS one* 7(6):e38011
115. Saalfeld S, Cardona A, Hartenstein V, Tomančák P. 2010. As-rigid-as-possible mosaicking and serial section registration of large sstem datasets. *Bioinformatics* 26(12):i57–i63
116. Yoo JC, Han TH. 2009. Fast normalized cross-correlation. *Circuits, systems and signal processing* 28:819–843
117. Liu Y, Lauderdale JD, Kner P. 2019. Stripe artifact reduction for digital scanned structured illumination light sheet microscopy. *Optics letters* 44(10):2510–2513
118. Rai MR, Li C, Greenbaum A. 2022. Quantitative analysis of illumination and detection corrections in adaptive light sheet fluorescence microscopy. *Biomedical Optics Express* 13(5):2960–2974
119. Foroosh H, Zerubia JB, Berthod M. 2002. Extension of phase correlation to subpixel registration. *IEEE transactions on image processing* 11(3):188–200
120. Preibisch S, Saalfeld S, Tomancak P. 2009. Globally optimal stitching of tiled 3d microscopic image acquisitions. *Bioinformatics* 25(11):1463–1465
121. Lowe DG. 2004. Distinctive image features from scale-invariant keypoints. *International journal of computer vision* 60:91–110
122. Schindelin J, Arganda-Carreras I, Frise E, Kaynig V, Longair M, et al. 2012. Fiji: an open-source platform for biological-image analysis. *Nature methods* 9(7):676–682
123. Swaney J, Kamentsky L, Evans NB, Xie K, Park YG, et al. 2019. Scalable image processing techniques for quantitative analysis of volumetric biological images from light-sheet microscopy. *BioRxiv* :576595
124. Saalfeld S, Fetter R, Cardona A, Tomancak P. 2012. Elastic volume reconstruction from series of ultra-thin microscopy sections. *Nature methods* 9(7):717–720
125. Hörl D, Rojas Rusak F, Preusser F, Tillberg P, Randel N, et al. 2019. BigStitcher: reconstructing high-resolution image datasets of cleared and expanded samples. *Nature methods* 16(9):870–874
126. Pietzsch T, Saalfeld S, Preibisch S, Tomancak P. 2015. BigDataViewer: visualization and processing for large image data sets. *Nature methods* 12(6):481–483
127. Renier N, Adams EL, Kirst C, Wu Z, Azevedo R, et al. 2016. Mapping of brain activity by automated volume analysis of immediate early genes. *Cell* 165(7):1789–1802
128. Ketcha MD, De Silva T, Han R, Uneri A, Vogt S, et al. 2019. A statistical model for rigid image registration performance: the influence of soft-tissue deformation as a confounding noise source. *IEEE transactions on medical imaging* 38(9):2016–2027
129. Bitplane. 2020. Imaris stitcher: Advanced image stitching for light sheet microscopy. *Imaris Software Package Documentation* Version 9.6
130. Abu Bakar ZH, Bellier JP, Wan Ngah WZ, Yanagisawa D, Mukaisho Ki, Tooyama I. 2023. Optimization of 3d immunofluorescence analysis and visualization using imaris and meshlab. *Cells* 12(2):218
131. Voigt FF, Kirschenbaum D, Platonova E, Pagès S, Campbell RA, et al. 2019. The mesospim initiative: open-source light-sheet microscopes for imaging cleared tissue. *Nature methods* 16(11):1105–1108
132. Maric D, Jahanipour J, Li XR, Singh A, Mobiny A, et al. 2021. Whole-brain tissue mapping toolkit using large-scale highly multiplexed immunofluorescence imaging and deep neural networks. *Nature communications* 12(1):1550
133. Park J, Wang J, Guan W, Gjesteby LA, Pollack D, et al. 2024. Integrated platform for multiscale molecular imaging and phenotyping of the human brain. *Science* 384(6701):eadh9979
134. Manders EM, Verbeek F, Aten J. 1993. Measurement of co-localization of objects in dual-colour confocal images. *Journal of microscopy* 169(3):375–382
135. Huisken J, Swoger J, Del Bene F, Wittbrodt J, Stelzer EH. 2004. Optical sectioning deep inside live embryos by selective plane illumination microscopy. *Science* 305(5686):1007–1009
136. Manders E, Stap J, Brakenhoff G, Driel Rv, Aten J. 1992. Dynamics of three-dimensional replication patterns during the s-phase, analysed by double labelling of dna and confocal microscopy. *Journal of cell science* 103(3):857–862

137. Li Q, Lau A, Morris TJ, Guo L, Fordyce CB, Stanley EF. 2004. A syntaxin 1, gαo, and n-type calcium channel complex at a presynaptic nerve terminal: analysis by quantitative immunocolocalization. *Journal of Neuroscience* 24(16):4070–4081
138. Moser B, Hochreiter B, Herbst R, Schmid JA. 2017. Fluorescence colocalization microscopy analysis can be improved by combining object-recognition with pixel-intensity-correlation. *Biotechnology journal* 12(1):1600332
139. Collins TJ. 2007. ImageJ for microscopy. *Biotechniques* 43(sup1):S25–S30
140. Costes SV, Daelemans D, Cho EH, Dobbin Z, Pavlakis G, Lockett S. 2004. Automatic and quantitative measurement of protein-protein colocalization in live cells. *Biophysical journal* 86(6):3993–4003
141. Lagache T, Sauvonnet N, Danglot L, Olivo-Marin JC. 2015. Statistical analysis of molecule colocalization in bioimaging. *Cytometry Part A* 87(6):568–579
142. Bolte S, Cordelières FP. 2006. A guided tour into subcellular colocalization analysis in light microscopy. *Journal of microscopy* 224(3):213–232
143. Ramirez O, Garcia A, Rojas R, Couve A, Härtel S. 2010. Confined displacement algorithm determines true and random colocalization in fluorescence microscopy. *Journal of microscopy* 239(3):173–183
144. Dunn KW, Kamocka MM, McDonald JH. 2011. A practical guide to evaluating colocalization in biological microscopy. *American Journal of Physiology-Cell Physiology*
145. Salinas CBG, Lu TTH, Gabery S, Marstal K, Alanentalo T, et al. 2018. Integrated brain atlas for unbiased mapping of nervous system effects following liraglutide treatment. *Scientific Reports* 8(1):10310
146. Wang X, Zeng W, Yang X, Zhang Y, Fang C, et al. 2021. Bi-channel image registration and deep-learning segmentation (birds) for efficient, versatile 3d mapping of mouse brain. *Elife* 10:e63455
147. Perens J, Salinas CG, Skytte JL, Roostalu U, Dahl AB, et al. 2021. An optimized mouse brain atlas for automated mapping and quantification of neuronal activity using idisco+ and light sheet fluorescence microscopy. *Neuroinformatics* 19(3):433–446
148. Spilger R, Lee JY, Bartenschlager R, Rohr K. 2022. *Deep neural network for combined particle tracking and colocalization analysis in two-channel microscopy images*. In *2022 IEEE 19th International Symposium on Biomedical Imaging (ISBI)*, pp. 1–4. IEEE
149. Kojima Y, Mii S, Hayashi S, Hirose H, Ishikawa M, et al. 2024. Single-cell colocalization analysis using a deep generative model. *Cell Systems* 15(2):180–192
150. Fürth D, Vaissière T, Tzortzi O, Xuan Y, Märtin A, et al. 2018. An interactive framework for whole-brain maps at cellular resolution. *Nature neuroscience* 21(1):139–149
151. Kornilov A, Safonov I, Yakimchuk I. 2022. A review of watershed implementations for segmentation of volumetric images. *Journal of Imaging* 8(5):127
152. Niyas S, Pawan S, Kumar MA, Rajan J. 2022. Medical image segmentation with 3d convolutional neural networks: A survey. *Neurocomputing* 493:397–413
153. Han K, Wang Y, Chen H, Chen X, Guo J, et al. 2022. A survey on vision transformer. *IEEE transactions on pattern analysis and machine intelligence* 45(1):87–110
154. Tyson AL, Rousseau CV, Niedworok CJ, Keshavarzi S, Tsitoura C, et al. 2021. A deep learning algorithm for 3d cell detection in whole mouse brain image datasets. *PLoS computational biology* 17(5):e1009074
155. Ducroz C, Olivo-Marin JC, Dufour A. 2012. *Characterization of cell shape and deformation in 3D using Spherical Harmonics*. In *2012 9th IEEE International Symposium on Biomedical Imaging (ISBI)*, pp. 848–851. IEEE
156. Son HJ, Kim S, Kim SY, Jung JH, Lee SH, et al. 2025. Three-dimensional β-amyloid burden correlation between the eye and brain in Alzheimer's disease mice using light-sheet fluorescence microscopy. *Investigative Ophthalmology & Visual Science* 66(3):34–34